Single cobalt atom anchored black phosphorous nanosheets as an effective cocatalyst promotes photocatalysis

Xiaohui Ren,[a, b] Li Shi,*[b] Yunxiang Li,[a, b] Shuang Song,[b, c] Qi Wang,[a, b] Shunqin Luo,[a, b] Long Ren,[d] Hongwei Zhang,[e] Yasuo Izumi,[e] Xinsheng Peng,[f] Davin Philo,[a, b] Fumihiko Ichihara,[a, b] Jinhua Ye*[a, b, g, h]

[a] X. Ren, Dr. Y. Li, Q. Wang, S. Luo, D. Philo, F. Ichihara, Prof. Dr. J. Ye
Graduate School of Chemical Sciences and Engineering
Hokkaido University
Kita 8, Nishi 5, Kita-ku
Sapporo 060-0814 (Japan)
[b] X. Ren, Dr. L. Shi, Dr. Y. Li, S. Song, Q. Wang, S. Luo, D. Philo, F. Ichihara, Prof. Dr. J. Ye
International Center for Materials Nanoarchitectonics (WPI-MANA)
National Institute for Materials Science (NIMS)
1-1 Namiki, Tsukuba
Ibaraki 305-0044 (Japan)
E-mail: SHI.Li@nims.go.jp (Dr. L. Shi); Jinhua.YE@nims.go.jp (Prof. Dr. J. Ye)
[c] S. Song
Department of Environmental Science and Engineering
School of Architecture and Environment
Sichuan University
Chengdu 610065 (P. R. China)
[d] Dr. L. Ren
Australia Institute for Superconducting and Electronic Materials (ISEM)
Australian Institute for Innovative Materials (AIIM)
University of Wollongong
Wollongong NSW 2500 (Australia)
[e] H. Zhang, Prof. Dr. Y. Izumi
Department of Chemistry
Graduate School of Science
Chiba University
Yayoi 1-33, Inage-Ku
Chiba 263-8522 (Japan)
[f] Prof. Dr. X. Peng
State Key Laboratory of Silicon Materials
School of Materials Science and Engineering
Zhejiang University
Hangzhou 310027 (P. R. China)
[g] Prof. Dr. J. Ye
TJU-NIMS International Collaboration Laboratory

School of Material Science and Engineering
Tianjin University
Tianjin 300072 (P. R. China)
[h] Prof. Dr. J. Ye
Collaborative Innovation Center of Chemical Science and Engineering (Tianjin)
Tianjin 300072 (P. R. China)

Abstract: Exploring novel cocatalysts with sufficient active sites and rapid photogenerated carrier separation remains challenge for boosting photocatalytic reaction. Recently, two-dimensional (2D) black phosphorus (BP) has been developed and recognized to be an ideal platform for anchoring metal ions through lone pair electrons. Herein, we propose a new structure that cobalt atomically dispersed on BP nanosheets (BP-Co), and apply it as cocatalyst for photocatalytic H_2 evolution and CO_2 reduction under visible light (>420 nm) irradiation. Both scanning transmission electron microscope and X-ray absorption near edge structure verified the existence of phosphorous-coordinated Co sites. The interaction between Co and P brings greatly improvement on photocatalytic activities, and 18-fold enhancement can be achieved on CdS when taking BP-Co as a noble-metal-free cocatalyst for H_2 evolution, which is higher than that of Pt under the same condition. Besides, BP-Co can also be used as an effective cocatalyst to promote photocatalytic CO_2 reduction in the presence of photosensitizer $[Ru(2, 2'\text{-bipyridy})_3]Cl_2$ with a CO evolution rate of 88.6 μmol h^{-1}, superior to those obtained from the state-of-the-art cocatalysts. It is anticipated that the current work might provide basic understanding as well as new opportunities on 2D BP nanosheets for versatile photocatalytic reactions.

Keywords: two-dimensional, black phosphorus, single atom, photocatalysis

1. Introduction

Photocatalytic reaction that can directly drill solar power is essential for next-generation portable and renewable energy applications.[1] To develop a high-efficient photocatalytic system, both photogenerated electron-hole pair separation efficiency and activation energy barrier on catalyst surface should be carefully taken into consideration.[2] Toward this end, cocatalysts with the abilities to retard charge carriers recombination and promote surface reactions are commonly used in various photocatalytic reactions such as water splitting, CO_2 reduction, etc.[3] Up to now, the searching for efficient cocatalysts becomes the utmost priority. Noble metals have been extensively investigated and metal Pt shows more favorite performance than other metals owing to its optimized work function and overpotential for H_2 evolution.[4] Unfortunately, considering the rarity and expensive cost of noble metals, the exploration of earth-abundant materials as the cocatalyst becomes indispensable.

To date, earth-abundant transition metals such as Co, Ni, Cu and their cluster show promising cocatalytic performance in various photocatalytic reactions.[5] Differing from other non-noble metals, Co possesses less 3d-orbital electrons and emerges as a promising catalyst for energy conversion and storage especially for H_2 evolution.[6] The existed cobalt can incorporate with semiconductor, by collecting electrons and providing effective active sites to enhance the ultimate photocatalytic performance in thermodynamics and kinetics aspects during catalytic process.[7] Recent advances indicate atomically dispersed metals (noted as single-atom metal) demonstrate remarkable catalytic activity owing to the strong size effect and enlarged surface exposed area.[8] It was reported that only small amount of single-atom metals loaded on C_3N_4 are necessary to induce a dramatically improvement of photocatalytic performance.[9] The high effectivity can be contributed to longer lifetime of photogenerated electrons in addition to favorable surface trap states because of the existence of single-atom metals.

Despite numerous merits of single-atom metals, the tendency of aggregation is usually unavoidable during fabrication processes.[10] Until now, several attempts successfully make an optimization to achieve stable single-atoms dispersion as well as high photocatalytic activity[11], while the strategy that applies coordinatively unsaturated material as supporting platform is considered to be the most feasible way in current situation. Recently, newly developed graphene-like semiconductor black phosphorous (BP) has gained considerable interests for photo-related

applications.[12] In the atomic structure of BP, only three of the five electrons in the outermost orbital are covalently bonded to each other, leaving the lone pair electrons to interact with metal ions. Apart from that, the relatively high carrier mobility in association with tunable direct bandgap together make it a promising substrate for stable catalyst dispersing.[13] Recent progress achieved by Bai and co-workers provided solid evidence on BP/Pt heterostructure for demonstrating enhanced stability as well as accelerated charge separation under the influence of strong BP-Pt interaction.[14] Meanwhile, Yuan et al. indicated the important role of Co-P bonds to facilitate charge-carrier transfer for efficient H_2 production.[15] Thereby, the adoption of BP nanosheets as the support material is deemed to trigger high stability and efficient electron-hole separation for atomically dispersed metals, prolonging the charge carrier lifetime and improving the photocatalytic reduction efficiency in consequence. In this regard, the integration of atomically dispersed metal Co with BP nanosheets substrate can be expected for realizing excellent photocatalytic activity. However, no related work has been reported as we known.

Herein, we prepared coordinated Co on BP nanosheets (BP-Co) as a cocatalyst and applied it into photocatalytic H_2 evolution and CO_2 reduction. The H_2 production performance evaluation reveals that BP-Co can dramatically improve the photocatalytic performance of CdS, reaching an attractive H_2 production rate of 345.4 μmol h^{-1} (18 times higher than that of pure CdS). Apart from that, BP-Co can also be used as an effective cocatalyst to promote photocatalytic CO_2 reduction in the presence of photosensitizer [Ru(2, 2'-bipyridy)$_3$]Cl_2 ([Ru]). The CO evolution rate reaches up to 88.6 μmol h^{-1}, superior to those results obtained from the state-of-the-art cocatalysts. We attribute the enhanced photocatalytic reduction performance into the atomically dispersed cobalt active sites and improved electron-hole separation efficiency through additional Co-P(O) charge transfer channel. By disclosing the ability of BP nanosheets for atomically dispersed cobalt anchoring, our results will provide a meaningful way for designing advanced BP based materials for efficient photocatalysis.

2. Results and discussion

BP nanosheets are produced from bulk BP crystal material by liquid exfoliation in 1-Methyl-2-pyrrolidone (NMP) solution as illustrated in Figure 1(a). Scanning electron microscopy (SEM) images show the exfoliated few-layer BP nanosheets preserved its layer structure while the thickness and size decrease obviously when compared to that of bulk BP crystals (Figure S1). X-

ray diffraction (XRD) patterns (Figure S2) show BP bulk and BP nanosheets can be indexed into orthorhombic BP crystalline structure in consistent with JCPDS No. 73-1358. A new diffraction peak (111) appears in the result of as-prepared BP nanosheets which formerly cannot be found in pristine bulk structure, and the peak intensity ratio between (021) and (040) also changes from (0.496/1) to (1.027/1). These slight deviations possibly resulted from the cleaving along with {010} facets of BP crystal during exfoliation process, as reported previously by other papers.[16] From High-resolution transmission electron microscopy (HRTEM) images (Figure S3 and Figure S4), the lattice spacing (d-spacing) of 0.33 nm and 0.246 nm corresponds to (021) and (040) plane of few-layer BP nanosheets, respectively. In addition, atomic force microscopy (AFM) analyses in Figure S5 confirm the lamellar structure which can be observed from TEM measurements. The thickness of as-prepared BP nanosheets ranges from 4 nm to 10 nm, which is corresponding to the value of few-layers BP nanosheets.[17] Average line analysis is preformed based on three-dimensional AFM height image, and the extracted height profile of exfoliated few-layer BP nanosheets is approximately 5 nm, indicating the successful preparation of BP nanosheets.

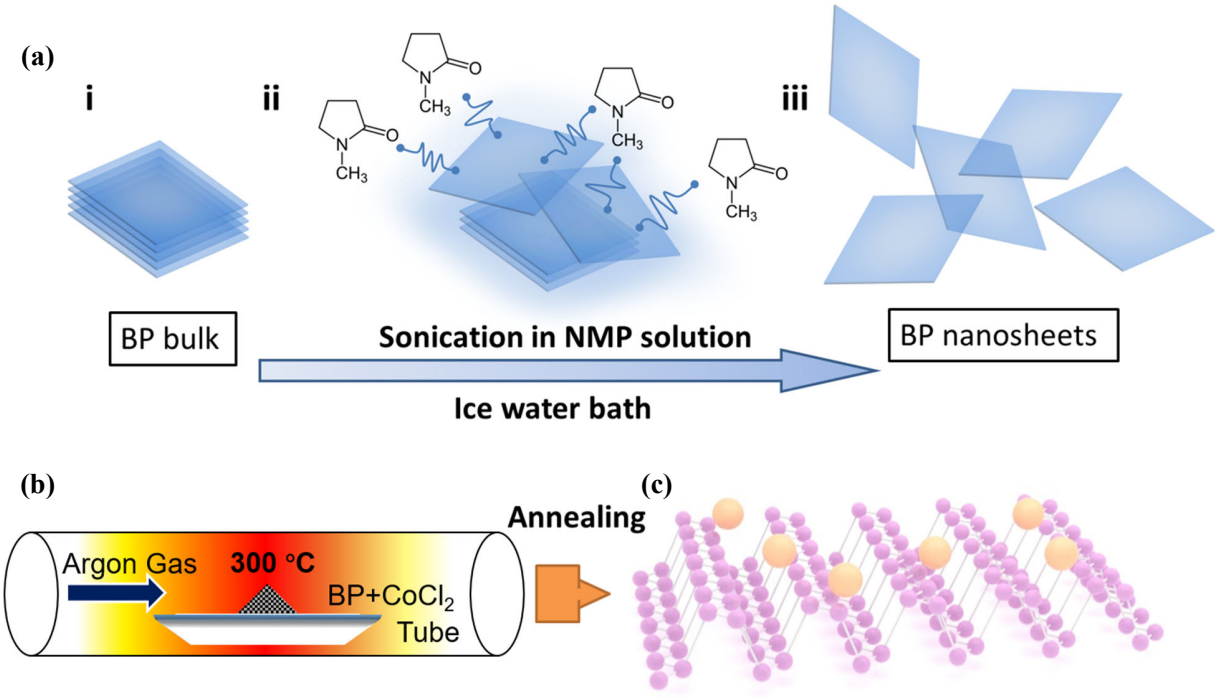

Figure 1. (a) Schematic illustration of NMP liquid solution assisted probe sonication exfoliation route in ice water bath to prepare few-layer BP nanosheets. (b) Proposed strategy to obtain uniform dispersed Co on BP nanosheets substrate. (c) Atomic structure of single atom dispersed BP nanosheets.

Figure 1(b) illustrates the proposed strategy to attach atomically dispersed Co onto the surface of BP nanosheets (Figure 1(c)). To further confirm the interaction between Co and BP, characterizations including TEM, high-angle annular dark-field STEM (HADDF-STEM), AFM and Zeta-potential are investigated (see supporting information **Experimental Section** for detail information). The low resolution TEM image (Figure 2(a)) reveals the typical morphology of layer BP nanosheets. HAADF-STEM image (Figure 2(b)) of BP-Co shows the high density bright dots (highlighted by red circles), which clearly depicts that the Co is atomically dispersed on the surface of BP, while the HRTEM image of the related area demonstrated in Figure 2(c) indicates good crystallization of BP nanosheets. Besides that, EDX spectroscopy (Figure S6) and mappings (Figure 2(d) and Figure S7) also indicate the existence of uniformly distributed Co element on BP nanosheets, while unavoidable oxidation and the use of $CoCl_2$ in synthesis processes maybe lead to the appearance of O and Cl elements. We notice that the layered structure and the lateral size of BP nanosheets remain intact after Co loading from SEM images (Figure S8). Meanwhile, the AFM measurement of BP-Co material reveals sheet-like structure and the thickness has nearly no change when compared to that of original BP layers (Figure 2(e) and Figure 2(f)). Zeta-potential measurements in Figure 2(g) indicate the surface charge on BP in solution, and exfoliated BP nanosheets shows the lowest average value of -26.6 mV, suggesting well distribution status than that of bulk BP. Meanwhile, zeta-potential becomes positive after Co modification, and increase from -26.6±0.48 mV for BP nanosheets to +21.9±0.26 mV for BP-Co. Both freshly prepared BP nanosheets and BP-Co materials show well dispersion in water and obvious Tyndall effect (inset image in Figure 2(g)). Those results emphasize the successful immobilization of Co onto the negatively charged BP nanosheets.

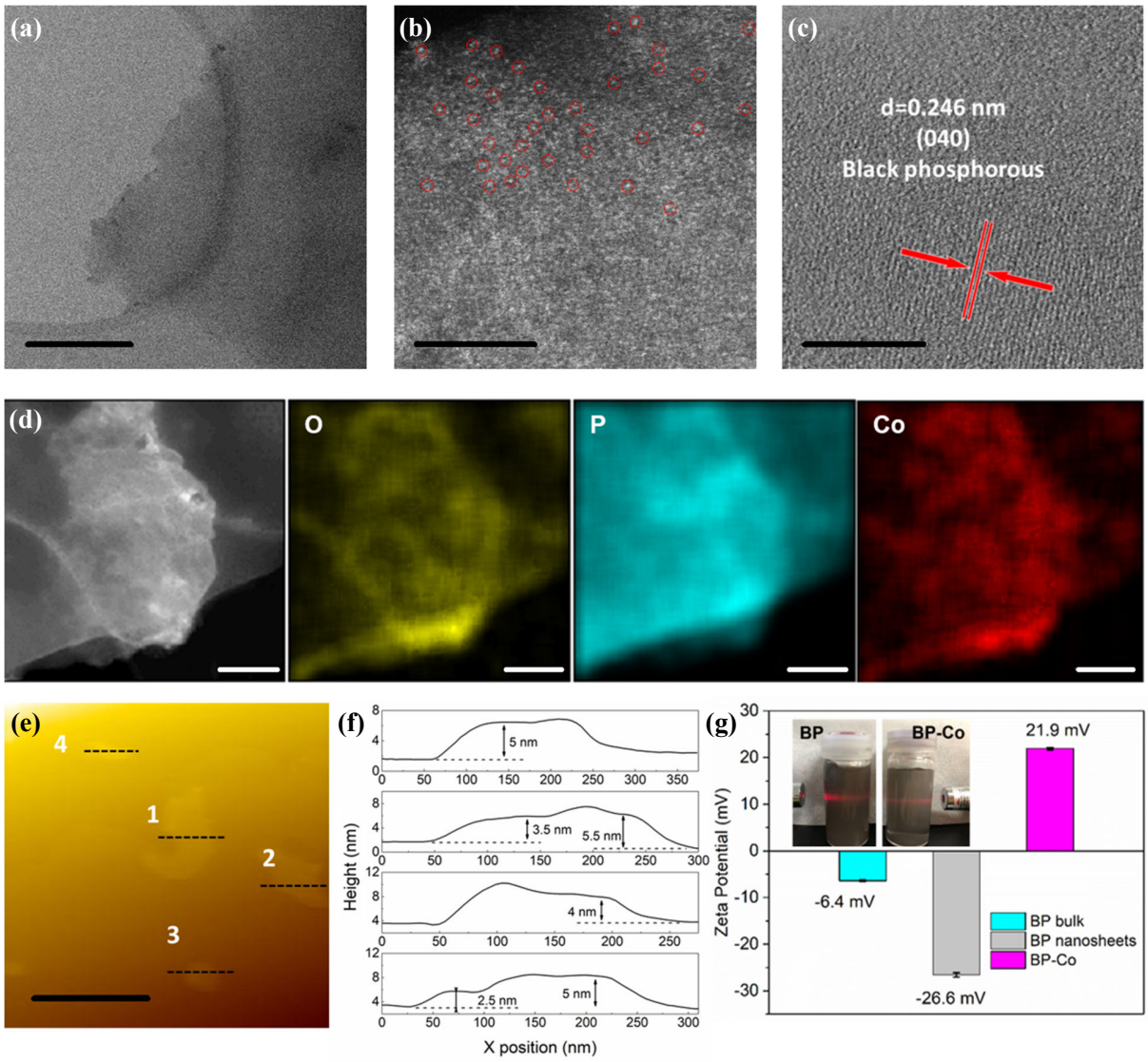

Figure 2. (a) Low resolution TEM (scale bar 100 nm), (b) HADDF-STEM (scale bar 5 nm) image (Co atoms are marked using red circles), (c) HRTEM image (scale bar 5 nm) with d-spacing 0.246 nm of BP-Co material. (d) EDS mapping images of as-prepared BP-Co material (scale bar 100 nm). (e) Tapping-mode AFM image (scale bar 500 nm) and (f) the related cross-sectional analysis (line 1 to line 4) of BP-Co. (g) Zeta-potential of BP bulk, freshly prepared BP nanosheets and BP-Co tested in ethanol solution. (Inset image: Observation of Tyndall effect of freshly prepared BP nanosheets and BP-Co dispersed in water.)

XRD patterns in Figure 3(a) shows no difference between fresh BP nanosheets and BP-Co, except for the ratio between (040) and (111) peaks appeared at 34.2° and 35° changes little. We suppose this phenomenon can reflect the interaction between lone pair electrons on the surface of

exposed BP nanosheets and Co ions. Raman spectra of BP nanosheets are shown in Figure 3(b). BP belongs to the Cmca (No. 64) space group, and in this situation both out-of-plane vibration A_g^1 mode as well as in-plane vibration B_{2g} and A_g^2 modes can be observed through Raman spectra analysis.[18] The position of Raman peaks A_g^1, B_{2g} and A_g^2 of as-exfoliated few-layer BP nanosheets downshift from its bulk counterpart position (Table S1) about 0.9 cm^{-1}, 2.1 cm^{-1}, and 3.3 cm^{-1} due to thickness decreasing as previously reported.[19] The light absorption capacities of BP and BP-Co have been determined by UV-Vis-NIR absorption spectra (Figure S9), the threshold value of 1078 nm and 1512 nm from intrinsic absorption edge of BP and BP-Co spectra corresponding to the bandgap of 1.15 eV and 0.82 eV, respectively. The narrowed band gap is believed to be induced by the increased carrier concentration from cobalt ions and the creation of defect levels (or mid-gap state) in the bandgap[20], which acting as trap sites to accommodate the photogenerated electrons and promote charge carrier migration in consequence. The band energy position of BP is determined by Mott-Schottky plot (Figure S10), and the flat band potential is determined to be -1.12 V vs. Ag/AgCl (-0.92 V vs. NHE). After coordinated with Co, the flat band potential will further downshift to be -1.01 V vs. Ag/AgCl (-0.81 V vs. NHE) (Figure S10). Considering the small difference between the flat band potential and conduction band (CB) position for n-type semiconductors, the band positions of BP and BP-Co are estimated (Figure S11). It indicates that CB positions of BP and BP-Co are much higher than H_2 production potential (-0.41 V vs. NHE). Also, the on/off photoresponse behaviors in Figure S12 show the photocurrent density of BP-Co is 10 times higher than that of BP nanosheets, and a much longer response time of BP-Co means a longer photogenerated carrier lifetime after Co coordination. EIS investigations (Figure S13) also reveal a smaller semicircular radius for BP-Co which represents improved conductivity and lower charge transfer barrier than that of BP nanosheets. Thus, introduce the Co may greatly shorten diffusion distance and realize efficient electron-hole separation to induce favorite photocatalytic reduction kinetics.

The chemical states of BP-Co as well as electronic interactions are studied by using X-ray photoelectron spectroscopy (XPS) analysis. For as-prepared BP nanosheets, binding energies at 129.8 eV, 131.0 eV and 133.7 eV can be assigned to P $2p_{3/2}$. P $2p_{1/2}$ and P_xO_y (P-O species) on the surface, respectively.[21] In comparison, the three predominated P 2p peaks (Figure 3(c)) shift to lower binding energies 129.3 eV, 130.6 eV and 133.1 eV, which indicates strong interaction between BP and Co. High resolution core-level Co 2p spectrum (Figure 3(d)) of BP-Co material

can be fitted with spin-orbit split $2p_{3/2}$ and $2p_{1/2}$ main peaks and two satellites. The binding energies of 781.7 eV, 786.0 eV, 797.0 eV and 803.4 eV can be attributed into Co^{2+} and Co^{3+} components due to unavoidable surface oxidation, the peak observed lower than 781.7 eV may suggest a new bond Co-P formed due to interaction between Co and P.[22] In all situations, standard C 1s peaks are used for calibration (Figure S14 and Figure S15).

In order to further understand the atomic structure of BP-Co, X-ray absorption near-edge structure (XANES) spectroscopy and Co K-edge extended X-ray absorption fine structure (EXAFS) spectrometry are used to probe the local structure of the Co element in BP-Co material. The Co K-edge XANES spectra of Co metal foil, CoO, CoP, and BP-Co are demonstrated in Figure 3(e). Different from the spectra of metallic Co and CoO reference materials, the as-fabricated BP-Co exhibits near edge structure which is very similar to that of CoP reference sample. The EXAFS data of BP-Co was Fourier transformed over R-space range (R range) up to 4.0 Å as shown in Figure 3(f), the Co metal foil and CoO exhibit typical Co-Co shell peak at 2.2 Å and Co(-O-)Co shell peak at 2.6 Å (both peaks phase shift uncorrected). For BP-Co sample, three peaks appeared in the R range between 0 and 4 Angstrom. While peak position due to Co-O (1.34 Å) and Co-P (1.68 Å) matched well with corresponding peaks of CoO and CoP reference samples, a peak at 2.06 Å does not match the peaks observed for Co metal, CoO, or CoP references and should be related to Co-Cl coordination from surface remained $CoCl_2$.[23] Both the XANES and EXAFS information reveal that the Co is coordinated with P after annealing, and no Co-Co peaks are observed which indicates the single-atom status of Co. The coordination number has been extracted from curve fit analyses as shown in Figure S16. In detail, the coordination number of cobalt to oxygen is calculated to be 3.9, and the value of cobalt to phosphorous atoms is close to 1.5 (Calculation methods are provided in supporting information). Considering the fact that P-O species existed on the surface of BP nanosheets, we predict one isolated Co atom is coordinated with one or two phosphorous atoms as well as four oxygen atoms to form Co-P(O) species in BP-Co atomic structure.

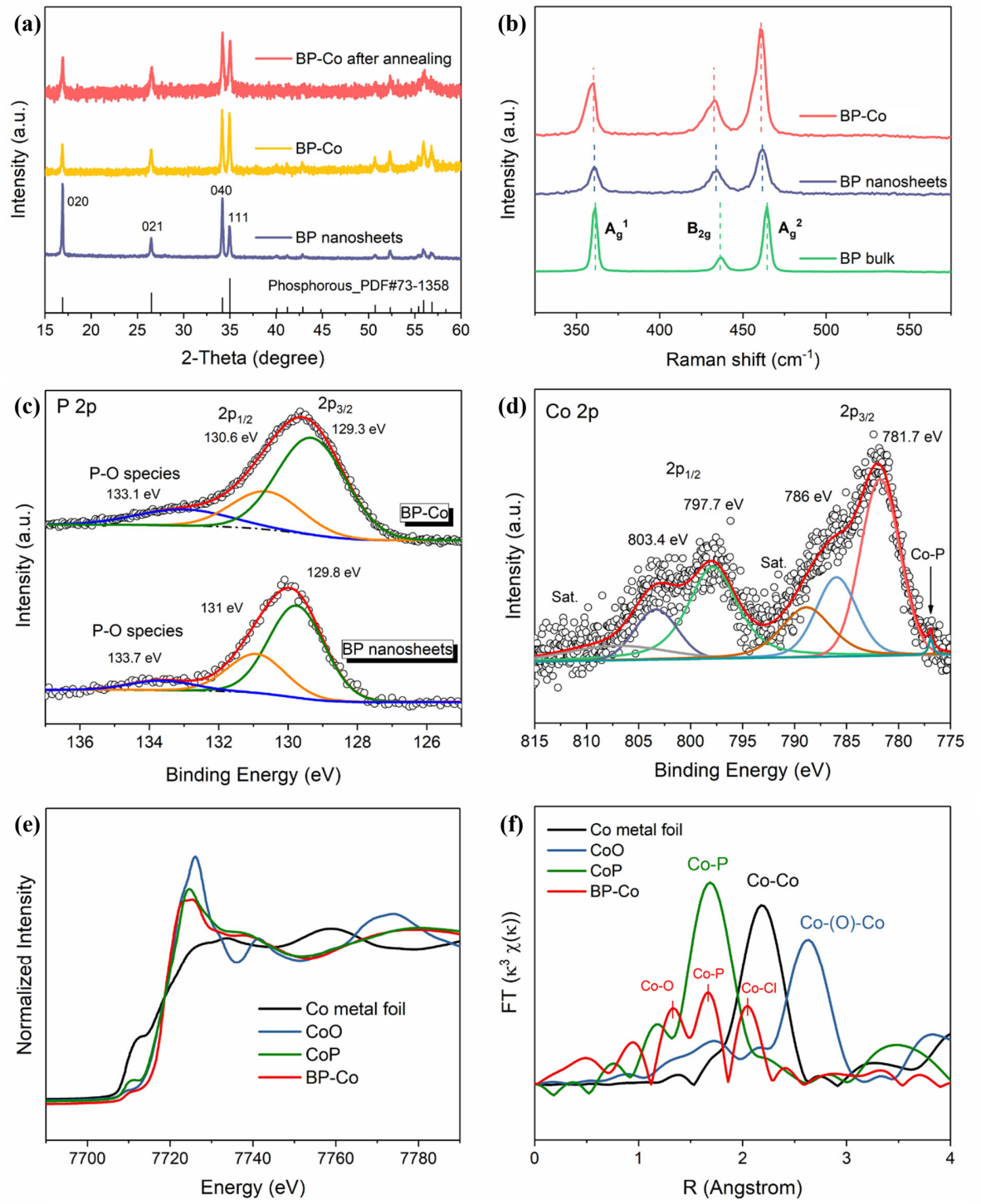

Figure 3. (a) XRD analysis of BP nanosheets and BP-Co before and after annealing process. (b) Raman spectra of BP bulk, BP nanosheets and BP-Co. (c) P 2p and (d) Co 2p binding energy spectra. (e) Co K-edge XANES spectra and (f) Fourier transform magnitudes of the experimental Co K-edge EXAFS spectra of BP-Co and reference samples.

An evidential improvement of photocatalytic reduction capability has been provided based on our experiments. The as-prepared BP-Co is chosen to combine with CdS for photocatalytic investigations. After combination, the absorption ability of CdS-BP-Co materials has been explored to NIR region, as shown in Figure S17. As shown in Figure 4(a), pure CdS possesses low photocatalytic H_2 production performance which is only 18.5 μmol h^{-1}. After mechanical mixing CdS with 0.5 wt% BP-Co, 5 times improvement can be achieved. The most optimized ratio between CdS and BP-Co is 1 wt%, and the average H_2 production rate is determined to be 345.4 μmol h^{-1}, which is 18 times higher than that of pure CdS. The H_2 production performance of the optimized CdS- 1% BP-Co can retain 90% from the first stage after three cycles (Figure S18). The promotion is basically from synergetic effect between BP and Co, for 1 wt% loading of BP will only achieve 3 times enhancement. In Figure 4(a) and Figure S19, the H_2 production rate of CdS with 1 wt% BP-Co is even higher than that of Pt at the same loading amount, and the performance is comparable with other reported BP based material in recent state (Table S2).[16, 21, 24] However, no H_2 evolution was observed over bare BP or BP-Co without the assistance of CdS, which we think it is because of the fast electrons and holes recombination in the situation of both BP and BP-Co (Figure S20). Our findings not only suggest the importance of BP nanosheets as a substrate for atomic metal loading, but also great potential of BP-Co as substitute for Pt cocatalyst for photocatalytic H_2 evolution.[25]

Based on our experimental results, the mechanism that views BP-Co in both band structure as well as surface interaction has been proposed in Figure 4(b) and (c). From the aspects of band structure of CdS-BP-Co, the CB edge of CdS (-1.03 eV vs. NHE) is higher than that of BP nanosheets (-0.92 eV vs. NHE) and BP-Co (-0.81 eV vs. NHE), a thermodynamic driving force will drive photogenerated electrons transfer from excited CdS to BP and Co-P(O) sites in the end. From the aspects of surface interaction, the intimate and large contact interface of CdS, BP and Co-P(O) give a new insight on the enhanced H_2 evolution activities. Generally, two different surface contact modes (face contact and point contact) play different roles in the charge carrier transport and chemical reactions. The face contact between BP nanosheets and CdS particles promotes fast charge transfer, improving electron-hole separation efficiency.[26] Meanwhile, the point contact between CdS and Co-P(O) leads to antenna effect, collecting electrons and lowering the energy barrier of photocatalytic reduction reactions. The active sites of BP-Co are further revealed by using photosensitizer Eosin Y to exclude the influence from semiconductor

CdS. (see supporting information for detail discussion, Figure S21-26) The H_2 production performances of BP, BP-Co and BP-$CoCl_2$ (BP-Co^{2+}) in Eosin Y system have been investigated. BP-Co demonstrates the highest activity and good stability (90 % from its pristine stage even after 1-week duration) amongst all reference samples. Thus, it is reasonable to believe the interaction between Co and P(O) on the surface may support uniform distribution of Co and provide additional charge transfer channel from CdS to Co-P(O) active sites to achieve improved photocatalytic performance.

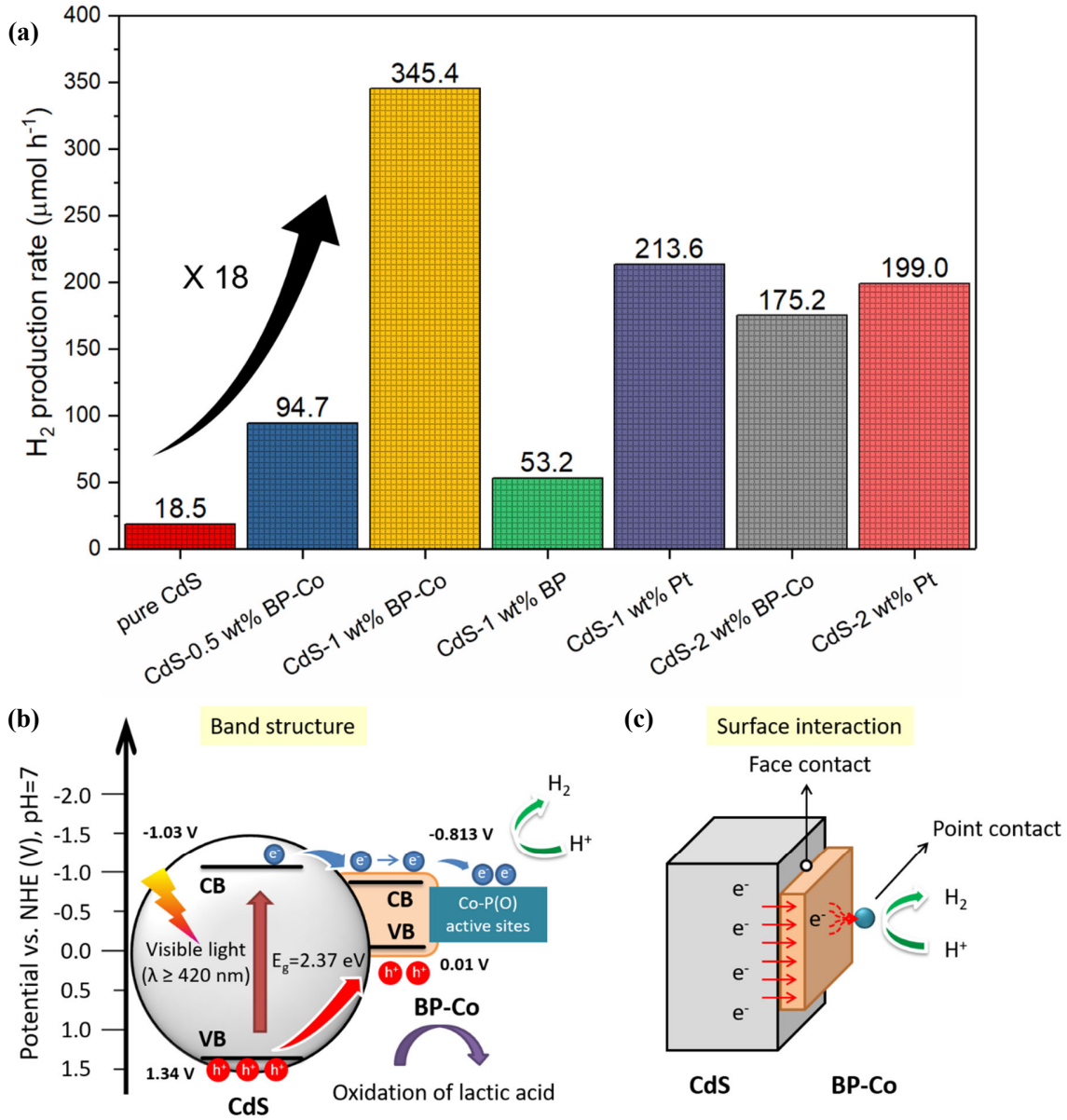

Figure 4. (a) Averaged H_2 evolution rate of pure CdS, CdS-0.5 wt% BP-Co, CdS-1 wt% BP-Co, CdS-1 wt% BP, CdS-2 wt% BP-Co, CdS-1 wt% Pt, and CdS-2 wt% Pt. (Catalyst amount: 20 mg). Schematic illustration on the (b) band structure and (c) surface interaction mechanism of photocatalytic reaction on CdS-BP-Co.

We further investigate the CO_2 reduction performance (Figure 5(a)) of BP-Co in CH_3CN, TEOA and water mixing solution saturated with atmospheric CO_2 in the presence of [Ru] as photosensitizer under visible light ($\lambda > 420$ nm). In detail, bare BP in the presence of [Ru] depicts excellent performance on water reduction to H_2, and nearly no CO can be detected means the CO_2 reduction is much harder kinetically than water reduction for bare BP. After Co loading, the H_2 reduction performance of BP slightly decreases, whereas the CO_2 reduction ability increases dramatically to 88.6 μmol h^{-1}, superior to those obtained with the state-of-the-art noble-metal-free cocatalysts (Table S3). [27] The CO_2 reduction performance we have achieved is 88.6 μmol h^{-1} for BP-Co with H_2 production of 61.1 μmol h^{-1} at the same time (Figure 5(b)), and the selectivity of CO is calculated to be 59.2% in consideration of the competition between water and CO_2 reduction. The excellent photocatalytic reduction performance of BP-Co may be triggered by the interaction between Co and P, which has been reported to show electron-rich property for boosting photocatalytic reactions.[28] The electron-rich property of BP-Co may lead to higher surface electron density for promoting photogenerated electrons to participate into the reactions with multiple electrons involved.[29] No CO evolution was observed over bare BP or BP-Co in the absence of [Ru], indicating the cocatalytic effect of BP and BP-Co for photocatalytic CO_2 reduction. Isotope experiments are carried out to validate the source of generated CO by using $^{13}CO_2$ as carbon source to replace $^{12}CO_2$ during our experiments. As shown in Figure 5(c), the total ion chromatographic peak around 6.2 minutes can be assigned to CO, while O_2 and N_2 are confirmed from air that remain in the sampling needle. The analysis of CO only obtains the m/z= 29 in mass spectra (Figure 5(c)), which is attributed to the ^{13}CO, confirming that the product CO originates from CO_2 reduction. The proposed mechanism for photocatalytic CO_2 reduction over BP-Co has been depicted in Figure 5(d). The photosensitizer [Ru] is excited under visible light to the [Ru]* state, and transferring generated electrons to the CB and the Co-P(O) active sites of BP-Co. Then, the CO_2 molecules and H^+ are reduced to CO and H_2. The oxidized state of the $[Ru]^+$ receives electrons from sacrificial electron donor TEOA to recover back to [Ru].

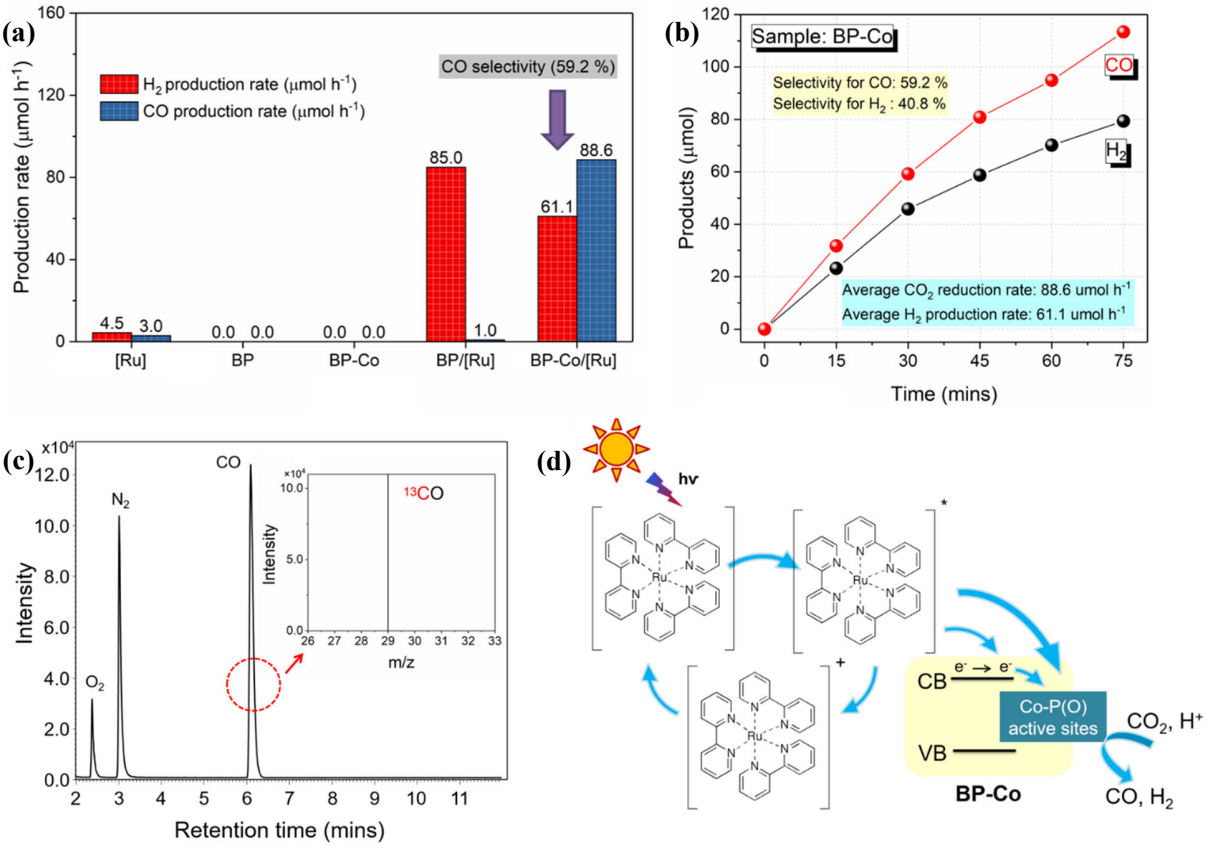

Figure 5. (a) Diagram of H_2 generation and CO_2 reduction performance of different catalysts. (b) Time dependent plot of BP-Co for CO_2 photocatalytic reduction with selectivity 59.2% in the presence of [Ru]. (c) GC-mass spectra of ^{13}CO (m/z = 29) produced over BP-Co/[Ru] from the atmosphere of $^{13}CO_2$. (d) The schematic illustration about the mechanism of electron transfer in BP-Co/[Ru] for photocatalytic CO_2 reduction.

3. Conclusion

In summary, we have prepared two-dimensional BP-Co nanostructure, where coordinated Co atoms are dispersed on the surface of BP nanosheets. The as-prepared BP-Co can be used as cocatalyst to enhance photocatalytic ability for both H_2 production and CO_2 reduction. We find that BP-Co loaded CdS can deliver much higher H_2 production performance than that of Pt loaded CdS, indicating great potential of BP-Co as substitute for Pt cocatalyst for photocatalytic H_2 evolution. On the other hand, the CO evolution rate as high as 88.6 μmol h^{-1} has been realized from photocatalytic CO_2 reduction over BP-Co in the presence of [Ru], superior to those obtained from the state-of-the-art noble-metal-free cocatalysts. Based on the results of

photocatalytic and photoresponse measurements, we attribute the enhancement of photocatalytic reduction to additional charge transfer channel and active sites derived from Co-P(O) bonding which can benefit photocatalytic conversion kinetics for boosting performance. In our work, the Co-P(O) interaction assist stable dispersion of single atom Cobalt on the surface of BP, leading BP-Co nano-materials with good activity as well as promising future in many photo-related applications including hydrogen generation, CO_2 reduction, pollutant degradation and photo-thermal reactions.

4. Methods

Materials. Black phosphorus (BP) bulk (99.5%) was provided by a commercial supplier (Nanjing XF NANO), 1-Methyl-2-pyrrolidinone (NMP) (99.5%, anhydrous), ethanol (95%) and $CoCl{\cdot}6H_2O$ (99.0%) were purchased from FUJIFILM Wako Pure Chemical Corporation. Tris(2, 2'-bipyridyl) dichlororuthenium(II) ($[Ru(2, 2'\text{-bipyridy})_3]Cl_2$, 99.95%) was purchased from Sigma-Aldrich Corporation. The deionized water with a resistivity of 18.2 $M\Omega\ cm^{-1}$ was utilized in all experiments.

Preparation of few-layer BP nanosheets. Few-layer BP nanosheets were obtained by using liquid exfoliation method. In detail, 0.5 g bulk BP was used as received and grinded in an agate mortar with the help of NMP. Then, a small portion of the pre-treated BP solution was transferred into a conical tube (50 mL) with totally 35 mL NMP added. The exfoliation processes are carried out in the micro-tip probe ultrasonication (Branson Sonifier advanced 250) with output power level 5 and duty cycle 50% at a temperature below 25 °C. After 3 hours' sonic exfoliation, the dispersion contains BP nanosheets can be harvested after several times centrifugation at 18000 rpm in order to remove the residual bulk BP. After that, the powder of BP nanosheets was retrieved after washing for three times using acetone and ethanol, and drying under 120 °C overnight for further characterizations.

Fabrication of BP-Co materials. In a typical experiment, the obtained BP nanosheets were mixed with $CoCl{\cdot}6H_2O$ directly. After grinding the aforementioned materials in an agate mortar for 15 minutes, the BP-Co precursor will be collected and transferred into a porcelain boat and located at the heating center of the quartz tube furnace. Before heating, the sealed quartz tube was pumped with argon gas for approximately 30 minutes to evacuate oxygen and air as much as possible. After the argon gas washing was finished, the furnace was heated to 300 °C with heat

speed 5 °C min^{-1} and maintain at this temperature for calcination for 2 hours. The final sample named as BP-Co was collected after it cooling down to room temperature and washed by Ethanol and deionized water for 3 times.

Photocatalytic H_2 evolution activity. Photocatalytic activities were evaluated by the hydrogen evolution from water under visible light irradiation. A 300 W xenon arc lamp equipped with a 420 nm cut-off filter (to remove light with a wavelength lower than 420 nm) was used as the visible light source. Commercial CdS and freshly prepared BP-Co were physically mixing together, and 20 mg of mixed sample was dissolved into 80 mL of 20 vol% lactic acids (electron donor) solution by sonication for 5 minutes, after that the solution was transferred into a quartz glass reaction cell and connect to a gas-closed system with a gas-circulated pump. The produced H_2 was recorded and analyzed by an online gas chromatograph (GC-8A, Shimadzu Corp., Ar carrier, TCD, Japan) with argon as the carrier gas. For evaluating the H_2 production performance of BP-Co, 10 mg of catalyst, 20 mg Eosin Y (EY) and 80 mL of 25 vol% TEOA were added in a quartz glass reaction cell that was connected to a gas-closed system with a gas-circulated pump. Before the irradiation, the reaction cell was evacuated to remove the air completely. The produced H_2 was analyzed by an online gas chromatograph (GC-8A, Shimadzu Corp., Ar carrier, TCD, Japan) with argon as the carrier gas.

Photocatalytic CO_2 reduction activity. The CO_2 photocatalytic reduction experiments were conducted in the same gas closed circulation system equipped with a glass reaction cell (upside quartz window). Before the measurements, 1.5 mg of catalyst powders and 30 mg [Ru(2, 2'-bipyridy)$_3$]Cl_2 were used and uniformly dispersed into 30 mL of CH_3CN/TEOA/water mixing solution (CH_3CN:TEOA:H_2O = 3:1:1), the gas closed reaction system was evacuated and then filled with 100 KPa of pure CO_2 gas. A 300 W Xe-lamp with a 420 nm cut-off filter was employed as the visible light source to drive the CO_2 photo-conversion. The gaseous products formed in the reaction were sampled and measured with a gas chromatograph (GC-14B, Shimadzu) equipped with a flame ionization detector (FID) according to the standard curves, while the generation of H_2 was measured with an online gas chromatograph (GC-8A, Shimadzu) with a TCD detector. Isotopic labeling experiment was performed by replacing CO_2 gas with ^{13}C-labeled $^{13}CO_2$ (The Linde Group, ^{13}C enrichment: >99 atom%) under same test conditions, and the final products were analyzed by gas chromatography-mass spectrometry (GC-MS).

Acknowledges

This work was financially supported by JSPS KAKENHI (JP18H02065), the World Premier International Research Center Initiative (WPI Initiative) on Materials Nanoarchitectonics (MANA), MEXT (Japan), Photoexcitonix Project in Hokkaido University, National Natural Science Foundation of China (Grant No. 21633004 and 51872091), National Key R&D Program of China (Grant No. 2018YFC190503), State Scholarship Fund by China Scholarship Council (CSC) (201808430219). This research used the JEOL JEM-ARM200F funded by the Australian Research Council (ARC)-Linkage, Infrastructure, Equipment and Facilities (LIEF) grant (LE120100104) located at the UOW Electron Microscopy Centre.

References

[1] a) Z. Zou, J. Ye, K. Sayama, H. Arakawa, *Nature* **2001**, *414*, 625-627; b) K. Chang, X. Hai, J. Ye, *Adv. Energy Mater.* **2016**, *6*, 1502555; c) Y. Yan, J. Chen, N. Li, J. Tian, K. Li, J. Jiang, J. Liu, Q. Tian, P. Chen, *ACS Nano* **2018**, *12*, 3523-3532.

[2] J. Ran, M. Jaroniec, S. Z. Qiao, *Adv. Mater.* **2018**, *30*, 1704649.

[3] a) K. Chang, Z. Mei, T. Wang, Q. Kang, S. Ouyang, J. Ye, *ACS Nano* **2014**, *8*, 7078-7087; b) H. Li, W. Tu, Y. Zhou, Z. Zou, *Adv. Sci.* **2016**, *3*, 1500389; c) X. Meng, L. Liu, S. Ouyang, H. Xu, D. Wang, N. Zhao, J. Ye, *Adv. Mater.* **2016**, *28*, 6781-6803; d) Y. Li, S. Ouyang, H. Xu, W. Hou, M. Zhao, H. Chen, J. Ye, *Adv. Funct. Mater.* **2019**, *29*, 1901024.

[4] J. Liu, Y. Li, X. Zhou, H. Jiang, H. G. Yang, C. Li, *J. Mater. Chem. A* **2020**, *8*, 17-26.

[5] a) H. Li, Y. Zhou, W. Tu, J. Ye, Z. Zou, *Adv. Funct. Mater.* **2015**, *25*, 998-1013; b) J. Twilton, C. C. Le, P. Zhang, M. H. Shaw, R. W. Evans, D. W. C. MacMillan, *Nat. Rev. Chem.* **2017**, *1*, 0052; c) G. Zhao, W. Zhou, Y. Sun, X. Wang, H. Liu, X. Meng, K. Chang, J. Ye, *Appl. Catal. B* **2018**, *226*, 252-257; d) Y. Li, J. Hao, H. Song, F. Zhang, X. Bai, X. Meng, H. Zhang, S. Wang, Y. Hu, J. Ye, *Nat. Commun.* **2019**, *10*, 2359; e) X. Zhang, A. Fu, X. Chen, L. Liu, L. Ren, L. Tong, J. Ye, *Catal. Today* **2019**, *335*, 166-172; f) H. Zhang, Y. Dong, S. Zhao, G. Wang, P. Jiang, J. Zhong, Y. Zhu, *Appl. Catal. B* **2020**, *261*, 118233.

[6] H. Fei, J. Dong, M. J. Arellano-Jiménez, G. Ye, N. D. Kim, E. L. G. Samuel, Z. Peng, Z. Zhu, F. Qin, J. Bao, M. J. Yacaman, P. M. Ajayan, D. Chen, J. M. Tour, *Nat. Commun.* **2015**, *6*, 8668.

[7] G. Zhao, Y. Sun, W. Zhou, X. Wang, K. Chang, G. Liu, H. Liu, T. Kako, J. Ye, *Adv. Mater.* **2017**, *29*, 1703258.

[8] a) H. Zhang, G. Liu, L. Shi, J. Ye, *Adv. Energy Mater.* **2018**, *8*, 1701343; b) Q. Zhao, W. Yao, C. Huang, Q. Wu, Q. Xu, *ACS Appl. Mater. Interfaces* **2017**, *9*, 42734-42741.

[9] G. Gao, Y. Jiao, E. R. Waclawik, A. Du, *J. Am. Chem. Soc.* **2016**, *138*, 6292-6297.

[10] X.-F. Yang, A. Wang, B. Qiao, J. Li, J. Liu, T. Zhang, *Acc. Chem. Res.* **2013**, *46*, 1740-1748.

[11] a) M. Moliner, J. E. Gabay, C. E. Kliewer, R. T. Carr, J. Guzman, G. L. Casty, P. Serna, A. Corma, *J. Am. Chem. Soc.* **2016**, *138*, 15743-15750; b) X. Fang, Q. Shang, Y. Wang, L. Jiao, T. Yao, Y. Li, Q. Zhang, Y. Luo, H. L. Jiang, *Adv. Mater.* **2018**, *30*, 1705112; c) K. Jiang, S. Siahrostami, T. Zheng, Y. Hu, S. Hwang, E. Stavitski, Y. Peng, J. Dynes, M. Gangisetty, D. Su, K. Attenkofer, H. Wang, *Energy Environ. Sci.* **2018**, *11*, 893-903.

[12] a) T. Sakthivel, X. Huang, Y. Wu, S. Rtimi, *Chem. Eng. J.* **2019**, *379*, 122297; b) X. Ji, Y. Kang, T. Fan, Q. Xiong, S. Zhang, W. Tao, H. Zhang, *J. Mater. Chem. A* **2020**, *8*, 323-333; c) Y. Tian, H. Wang, H. Li, Z. Guo, B. Tian, Y. Cui, Z. Li, G. Li, H. Zhang, Y. Wu, *J. Mater. Chem. A* **2020**, *8*, 4647-4676.

[13] a) L. Kong, Y. Ji, Z. Dang, J. Yan, P. Li, Y. Li, S. Liu, *Adv. Funct. Mater.* **2018**, *28*, 1800668; b) F. Shi, Z. Geng, K. Huang, Q. Liang, Y. Zhang, Y. Sun, J. Cao, S. Feng, *Adv. Sci.* **2018**, *5*, 1800575.

[14] L. Bai, X. Wang, S. Tang, Y. Kang, J. Wang, Y. Yu, Z. K. Zhou, C. Ma, X. Zhang, J. Jiang, P. K. Chu, X.-F. Yu, *Adv. Mater.* **2018**, *30*, 1803641.

[15] Y.-J. Yuan, Z.-K. Shen, S. Song, J. Guan, L. Bao, L. Pei, Y. Su, S. Wu, W. Bai, Z.-T. Yu, Z. Ji, Z. Zou, *ACS Catal.* **2019**, *9*, 7801-7807.

[16] M. Zhu, S. Kim, L. Mao, M. Fujitsuka, J. Zhang, X. Wang, T. Majima, *J. Am. Chem. Soc.* **2017**, *139*, 13234-13242.

[17] M. Zhu, Y. Osakada, S. Kim, M. Fujitsuka, T. Majima, *Appl. Catal. B* **2017**, *217*, 285-292.

[18] D. J. Late, *ACS Appl. Mater. Interfaces* **2015**, *7*, 5857-5862.

[19] a) X. Ren, Z. Li, Z. Huang, D. Sang, H. Qiao, X. Qi, J. Li, J. Zhong, H. Zhang, *Adv. Funct. Mater.* **2017**, *27*, 1606834; b) W. Tao, X. Zhu, X. Yu, X. Zeng, Q. Xiao, X. Zhang, X. Ji, X. Wang, J. Shi, H. Zhang, L. Mei, *Adv. Mater.* **2017**, *29*, 1603276.

[20] W. Liu, L. Cao, W. Cheng, Y. Cao, X. Liu, W. Zhang, X. Mou, L. Jin, X. Zheng, W. Che, *Angew. Chem. Int. Ed.* **2017**, *56*, 9312-9317.
[21] L. Mao, X. Cai, S. Yang, K. Han, J. Zhang, *Appl. Catal. B* **2019**, *242*, 441-448.
[22] Q. Liang, F. Shi, X. Xiao, X. Wu, K. Huang, S. Feng, *ChemCatChem* **2018**, *10*, 2179-2183.
[23] a) J. Mizuno, *J. Phys. Soc. Jpn.* **1960**, *15*, 1412-1420; b) D.-H. Ha, L. M. Moreau, C. R. Bealing, H. Zhang, R. G. Hennig, R. D. Robinson, *J. Mater. Chem.* **2011**, *21*, 11498-11510; c) F. H. Saadi, A. I. Carim, W. S. Drisdell, S. Gul, J. H. Baricuatro, J. Yano, M. P. Soriaga, N. S. Lewis, *J. Am. Chem. Soc.* **2017**, *139*, 12927-12930.
[24] J. Ran, B. Zhu, S. Z. Qiao, *Angew. Chem. Int. Ed.* **2017**, *56*, 10373-10377.
[25] a) T. Simon, M. T. Carlson, J. K. Stolarczyk, J. Feldmann, *ACS Energy Lett.* **2016**, *1*, 1137-1142; b) L. Ma, K. Chen, F. Nan, J.-H. Wang, D.-J. Yang, L. Zhou, Q. Q. Wang, *Adv. Funct. Mater.* **2016**, *26*, 6076-6083; c) Q. Li, F. Zhao, C. Qu, Q. Shang, Z. Xu, L. Yu, J. R. McBride, T. Lian, *J. Am. Chem. Soc.* **2018**, *140*, 11726-11734.
[26] Y.-J. Yuan, P. Wang, Z. Li, Y. Wu, W. Bai, Y. Su, J. Guan, S. Wu, J. Zhong, Z.-T. Yu, Z. Zou, *Appl. Catal. B* **2019**, *242*, 1-8.
[27] a) S. Wang, W. Yao, J. Lin, Z. Ding, X. Wang, *Angew. Chem. Int. Ed.* **2014**, *53*, 1034-1038; b) C. Gao, Q. Meng, K. Zhao, H. Yin, D. Wang, J. Guo, S. Zhao, L. Chang, M. He, Q. Li, H. Zhao, X. Huang, Y. Gao, Z. Tang, *Adv. Mater.* **2016**, *28*, 6485-6490; c) K. Zhao, S. Zhao, C. Gao, J. Qi, H. Yin, D. Wei, M. F. Mideksa, X. Wang, Y. Gao, Z. Tang, R. Yu, *Small* **2018**, *14*, 1800762; d) Y. Li, J. Ren, S. Ouyang, W. Hou, T. Petit, H. Song, H. Chen, D. Philo, T. Kako, J. Ye, *Appl. Catal. B* **2019**, *259*, 118027; e) Y. Wang, S. Wang, X. W. Lou, *Angew. Chem. Int. Ed.* **2019**, *58*, 17236-17240; f) H. X. Zhang, Q. L. Hong, J. Li, F. Wang, X. Huang, S. Chen, W. Tu, D. Yu, R. Xu, T. Zhou, J. Zhang, *Angew. Chem.* **2019**, *131*, 11878-11882.
[28] P. Zhou, Q. Zhang, Z. Xu, Q. Shang, L. Wang, Y. Chao, Y. Li, H. Chen, F. Lv, Q. Zhang, L. Gu, S. Guo, *Adv. Mater.* **2020**, *32*, 1904249.
[29] J. Fu, K. Jiang, X. Qiu, J. Yu, M. Liu, *Mater. Today* **2020**, *32*, 222-243.

Entry for the Table of Contents

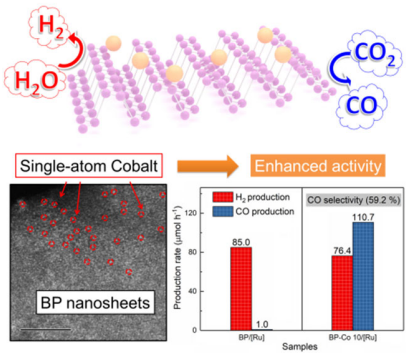

A new structure that cobalt atomically dispersed on BP nanosheets (BP-Co) has been realized, and applied as a noble metal-free cocatalyst for photocatalytic H_2 evolution and CO_2 reduction under visible light (>420 nm) irradiation. In this work, the photocatalytic reduction performance increased dramatically due to additional charge transfer channel and active sites derived from Co-P(O) interaction.